Perturbation Analysis of Thomas and Windle's Model of Case II Transport

C. J. Durning
Dept. of Chemical Engineering, Materials Science and Mining, Columbia University, New York, NY 10027

D. A. Edwards
Dept. of Mathematics, University of Maryland, College Park, MD 20742

D. S. Cohen
Applied Mathematics, California Institute of Technology, Pasadena, CA 91125

Thomas and Windle's model of Case II transport is analyzed for a semiinfinite medium by a singular perturbation technique. Two adjacent boundary layers separate equilibrated and dry regions. A thin boundary layer of width $\sim O(M^{-1/2}/\ln M)$, *where* M $(\gg 1)$ *dictates how rapidly the mixture's viscosity decays with liquid concentration, sits next to the equilibrated outer left region. Here, quasi-steady diffusion balances relaxation. A thicker intermediate layer of width* $\sim O(M^{-1/2})$ *separates the lefthand boundary layer and the dry outer region on the right, where both relaxation and unsteady diffusion participate in the transport. Matching the solutions at leading order specifies the moving front's speed,* v: $v \sim M^{1/2}$. *The analysis indicates that relaxation significantly affects the nearly dry region just ahead of the moving front. This disagrees with the widely accepted view that ordinary diffusion dominates in the nearly dry righthand region. Approximating that ordinary diffusion dominates in this region leads to a step-exponential concentration profile at the front and a simple analytical solution for the front speed,* v *with the correct* M *scaling. This approximate result accurately predicts the values of* v *determined by direct numerical solutions.*

Introduction

The unsteady diffusion of liquids in polymers is a controlling physical process in many engineering applications. Two examples are a class of control release devices, in which a bioactive species entrapped in a dense polymer matrix is slowly released by the progressive swelling of the matrix in an environmental fluid and certain barrier materials, which must effectively confine a liquid after initial contact on one side for an extended length of time. In these examples, and many others, simple mathematical models for the unsteady mass transport are invaluable design tools.

Unsteady interdiffusion in such systems is often complicated by viscoelastic or anelastic effects. Essentially, the polymer's response to its local dynamic history influences the mass transfer. This is shown in simple diffusion experiments, such as sorption or permeation, as obvious deviations from the predictions of Fick's laws (Vrentas and Duda, 1986). For unsteady diffusion over macroscopic length scales [$O(10^{-3} - 10^{-2}$ m)] such deviations appear inevitably when the system is near or below the glass transition since, under these conditions, the characteristic material time for the polymer becomes comparable to the relevant (macroscopic) time scale for the unsteady transport. In addition, such diffusion processes are often nonlinear in the sense that enormous changes in the governing transport properties accompany typical changes in local liquid content during the diffusion. In examples cited above, glassy polymers are employed and relatively large changes in composition occur during transport. Consequently, nonlinear "viscoelastic" or "anelastic" diffusion is encountered, showing striking deviations from Fick's laws.

Nonlinear, non-Fickian diffusion is difficult to model from first principles for two reasons. First, there is no widely accepted theoretical result telling precisely how material memory or anelasticity influences the diffusion flux in situations of practical importance. A second difficulty is the mathemati-

cal challenge of typical *initial value* problems derived from a first-principles model. Typical problems require numerical computation, which makes comparison with data cumbersome.

The objective of this work is to explore the predictions of a relatively simple nonlinear model for a striking non-Fickian effect, Case II transport. The model, first derived by Thomas and Windle (1982) from phenomenological arguments, was shown by Fu and Durning (1993) to be the small Deborah number limit of a more general theory for viscoelastic media derived from nonequilibrium thermodynamics (Durning and Tabor, 1986). We analyze this nonlinear model by a singular perturbation method to obtain a simple expression for the most important dynamic feature of the Case II process, the front speed. The phenomenology of Case II transport is discussed briefly, as well as the essentials of Thomas and Windle's (TW) model. Subsequently, the surface boundary condition in the model is analyzed, and then the diffusion equation is studied by a perturbation analysis.

Case II Transport and the TW Model

Alfrey, Gurnee and Lloyd (1966) documented unusual phenomenology during the unsteady sorption of liquid swelling agents in glassy polymers under immersion conditions. The striking observation was of a sharp liquid concentration front, separating highly swollen polymer from a nearly dry interior, propagating slowly into the sample *at constant speed*. At the same time the liquid mass uptake increased linearly with time. Neither observation can be reconciled with Fick's laws. Indeed the character of the process was so distinct from that normally associated with diffusion, Alfrey et al. labeled it Case II transport and proposed that it was a transport mechanism unique to polymer/fluid mixtures which becomes dominant in the glassy state.

Careful experiments have since clarified the phenomenology of Case II transport. Direct measurements of concentration profiles (Thomas and Windle, 1978; Hui et al., 1987a,b; Lasky et al., 1988) show that the fluid concentration at the polymer surface relaxes autocatalytically after first contact with the fluid, causing an initial delay or induction time in the liquid weight uptake kinetics. After the initial surface relaxation, a sharp liquid concentration profile develops and propagates into the sample at constant speed. Studies of sample thickness and temperature effects (Hopfenberg, 1978; Thomas and Windle, 1978) show that the front propagation can become limited by diffusion in the swollen region if the diffusion path length between the polymer/fluid interface and the front becomes large enough, or, equivalently, if the front speed becomes sufficiently large as occurs if one elevates the sorption temperature. Indirect evidence strongly suggests that Case II is a nonlinear effect, since it is not seen in "differential" sorption experiments (Billovits and Durning, 1990, 1993, 1994) where the composition change during transport is deliberately kept small so as to minimize or eliminate significant variations in physical properties during the process. In summary, the experimental evidence indicates that Case II is a particular manifestation of viscoelasticity or anelasticity in diffusion, appearing in sorption experiments when the composition dependence of transport properties is strong and fluid diffusion in the swollen surface layers is sufficiently rapid.

These experimental results have stimulated many modeling efforts. Thomas and Windle (1982) proposed a one-dimensional nonlinear model from phenomenological arguments which was shown by numerical solution and subsequent analysis (Hui et al., 1987a,b) to describe the essential character of Case II. Fu and Durning (1993) showed that the diffusion flux in the Thomas and Windle model can be derived by keeping the first nontrivial term in a retarded-motion expansion of a memory integral appearing in a more general flux law for diffusion in viscoelastic media. This approximation is only valid when the local diffusion Deborah number $De(c)$ is sufficiently small, where De gives the ratio of the local relaxation time for memory effects $\tau(c)$ to an external time scale for the unsteady diffusion. The Thomas and Windle flux law is

$$j_{1,\xi}^{2} = -D(c)\frac{\partial c}{\partial \xi} - D'(c)\frac{\partial}{\partial \xi}\left(\frac{\eta(c)}{G_o}\frac{\partial c}{\partial t}\right); \quad De(c) \ll 1 \quad (1)$$

where $j_{1,\xi}^{2}$ means the mass flux of liquid (component 1) relative to polymer (component 2) along the (material) coordinate ξ (Billovits and Durning, 1989). Also, c is the liquid mass concentration per unit volume of polymer, $D(c)$ is the polymer-material diffusion coefficient, $\eta(c)$ is the mixture's (zero shear rate) viscosity, and G_o is the dry polymer's high frequency shear modulus. The function $D'(c)$, scaling the contribution of memory effects to the flux, is proportional to $D(c)$ and to the ratio of G_o to the mixture's osmotic modulus (Durning and Tabor, 1986). If simple thermostatic behavior is assumed (Fu and Durning, 1993), one finds

$$D'(c) = \left(\varphi_{1e}\frac{\tilde{V}_1 G_o}{RT}\right)\left(\frac{c}{c_e}\right)D(c) \equiv D_o'\left(\frac{c}{c_e}\right)\left(\frac{D}{D_o}\right) \quad (2)$$

where c_e and φ_{1e} are the equilibrium values of the liquid concentration and volume fraction, respectively. Also, $\tilde{V}_1$ means the liquid molar volume, R is the gas constant, T is the absolute temperature, and $D_o = D(c=0)$.

Combining Eq. 1 with a 1-D liquid mass balance yields a third-order, nonlinear diffusion equation governing the liquid concentration field. For sorption, the appropriate boundary condition on the polymer/fluid interface is of continuity in the liquid chemical potential; the form thermodynamically consistent with Eqs. 1 and 2 is

$$\frac{RT}{\tilde{V}_1}\ln\frac{c}{c_e} + \varphi_{2e}\hat{V}_1\eta(c)\frac{\partial c}{\partial t} = 0 \quad (3)$$

where $\hat{V}_1$ means the liquid specific volume. The first term on the left approximates the thermostatic chemical potential for a given value of c; the second term on the left approximates the nonequilibrium contribution to the chemical potential because of the polymer's fading memory.

In Fu and Durning (1993) the diffusion equation for c based on Eqs. 1 and 2 was solved numerically for integral sorption in a dry thin film. Equation 3 gave the boundary conditions on the film surfaces and the representations $D(c) = D_o \exp(kc)$ and $\eta(c) = \eta_o \exp(-mc)$ were used. Three parameters appeared in the dimensionless initial value problem

$$\theta = \frac{\varphi_{1e}\tilde{V}_1\eta_o D_o}{RTl^2}; \quad K = kc_e; \quad M = mc_e.$$

θ is a Deborah number; K and M gauge the strength of nonlinearities in the problem; K measures how rapidly the diffusion coefficient increases with concentration while M measures how rapidly the viscosity decays with concentration. Estimates of these for 1-mm thick films of poly(methyl methacrylate) immersed in liquid methanol at room temperature, where Case II dominates, showed $\theta \sim O(10^{-2})$, $K \simeq M \sim O(10)$.

The numerical simulations by Fu and Durning (1993) revealed the following:

i. Both K and M must be sufficiently large (> 3) for Case II to be predicted from the model.

ii. θ must be small ($\sim O(10^{-2})$) for Case II to be predicted; however, Case II characteristics are extinguished for excessively small θ ($\ll 10^{-2}$).

iii. When Case II is predicted, the dimensionless front speed v obeys $v \sim \theta^{-1/2}$ for fixed values of K and M.

iv. When Case II is predicted, v increases monotonically with M for fixed K and θ; an unambiguous functional representation was not found however.

v. When Case II is predicted, the nonequilibrium contribution to the chemical potential $\sim \eta(c)\partial c/\partial t$ (see Eq. 3) forms a sharp, symmetric peak traveling at speed v just ahead of the liquid concentration front; it is nearly zero away from the front.

The last feature clarifies the role of fading memory in Case II through the effect of the nonequilibrium, relaxing part of the chemical potential. Evidently, relaxation effects are confined to a narrow spatial locus traveling at speed v; within this zone, $\eta(c)\partial c/\partial t$ is strongly peaked. On the side of its peak nearer the liquid reservoir, $\eta(c)\partial c/\partial t$ has a large positive slope, and so strongly retards diffusion of the fluid; this confines spreading of the liquid, causing it to collect at a sharp front immediately adjacent to the locus of relaxation.

1-D Sorption in Semiinfinite Medium

For mathematical convenience we study the Thomas and Windle model for sorption into a semiinfinite body of dry polymer. Let the polymer/fluid interface be located at $\xi = 0$. Then, defining scaled concentration $u \equiv c/c_e$, scaled distance $x \equiv \xi/(D_o'\eta_o/G_o)^{1/2}$ and scaled time $s \equiv t/(D_o'\eta_o/G_o D_o)$ leads to the dimensionless initial value problem

$$u_s = (e^{Ku}u_x)_x + [ue^{Ku}(e^{-Mu}u_s)_x]_x \quad \text{for} \quad \begin{cases} 0 < s < \infty \\ 0 < x < \infty \end{cases}, \quad (4)$$

$$u_s + e^{Mu}\ln u = 0 \quad \text{at} \quad x = 0 \quad \text{for} \quad 0 < s < \infty, \quad (5)$$

$$u \to 0 \quad \text{as} \quad x \to \infty \quad \text{for} \quad 0 < s < \infty, \quad (6)$$

$$\pi \equiv e^{-Mu}u_s \to 0 \quad \text{as} \quad x \to \infty \quad \text{for} \quad 0 < s < \infty \quad (7)$$

$$u = 0 \quad \text{at} \quad s = 0 \quad \text{for} \quad 0 \le x < \infty \quad (8)$$

$$\pi = 0 \quad \text{at} \quad s = 0 \quad \text{for} \quad 0 < x < \infty. \quad (9)$$

Equations 5–7 are the boundary conditions for the semiinfinite media; Eq. 7 expresses that the (dimensionless) nonequilibrium contribution to the chemical potential π vanishes far into the polymer, where the material is undisturbed. Equations 8 and 9 are the initial conditions of dry polymer at equilibrium.

Now, from the finding (i) in the numerical work mentioned above, we want both K and M to be large; hence, we let $K = \alpha M$ where $\alpha \sim O(1)$ and pursue an analysis for large M.

Analysis of Surface Boundary Condition

Equation 5 indicates that the fluid concentration at the polymer-fluid interface $u(x = 0, s)$ is not constant, but relaxes with time to the final, equilibrium value. We show that this relaxation becomes autocatalytic for large M. The governing equation already suggests this tendency. Figure 1 shows u_s vs. u according to Eq. 5 for various values of M. For large values of M the maximum becomes very sharply peaked and lies close to $u = 1$ (Figure 1b). The behavior suggests that for $M \gg 1$, $u(x = 0, s)$ should increase slowly at first, but later suddenly increase quite rapidly before abruptly skidding into the equilibrium value $u = 1$.

The exact solution of Eq. 5 is

$$\int_0^u \frac{e^{-My}}{\ln y}dy = -s. \quad (10)$$

Figure 2 shows the numerical evaluation of Eq. 10 by Romberg integration, using a finite lower limit to avoid numerical overflow. For large M, an autocatalytic response is clearly seen: $u(x = 0, s)$ rises slowly until an abrupt increase to 1 at a characteristic time $s*$ which appears to scale near $s* \sim M^{-1}$.

A short-time asymptote to Eq. 10, valid for large M and u such that $u \sim o(M^{-1})$, follows from Eq. 5, $u_s + \ln u \simeq 0$, which has the solution

$$E_1(\ln(1/u)) = s; \quad u \sim o(M^{-1}); \quad M \gg 1 \quad (11)$$

where $E_1 \equiv \int_x^\infty (e^{-x}/x)dx$. Since Eq. 11 is only good for s such that $u \sim o(M^{-1})$ and since $E_1(x) \sim e^{-x}/x$ for $x \gg 1$ (Gautschi and Cahill, 1965), Eq. 11 is only valid for $s \sim o(M^{-1}/\ln M)$, after which a rapid blowup in u occurs (e.g., Figure 2b). This blowup is logarithmic in s for large M, which can be seen by considering $u > O(M^{-1})$ but $\sim o(1)$. Putting $u = M^{-1}\bar{u}$ in Eq. 5 gives

$$\bar{u}_s + Me^{\bar{u}}(\ln\bar{u} - \ln M) = 0.$$

In the regime of interest, the second of the logarithm terms dominates and we have

$$u = \frac{1}{M}\ln\left(\frac{1}{\bar{s}_o - sM\ln M}\right); \quad u\begin{cases} > O(M^{-1}) \\ \sim o(1) \end{cases}; \quad M \gg 1 \quad (12)$$

where $\bar{s}_o \sim O(1)$ is an integration constant.

The asymptotic approach of u to its equilibrium value can also be understood from Eq. 5. Consider when $u = 1 - \Delta/M$, with $\Delta \sim O(1)$. For $M \gg 1$, Eq. 5 becomes

$$\Delta_{\hat{s}} + e^{\Delta}\Delta \simeq 0 \quad (13)$$

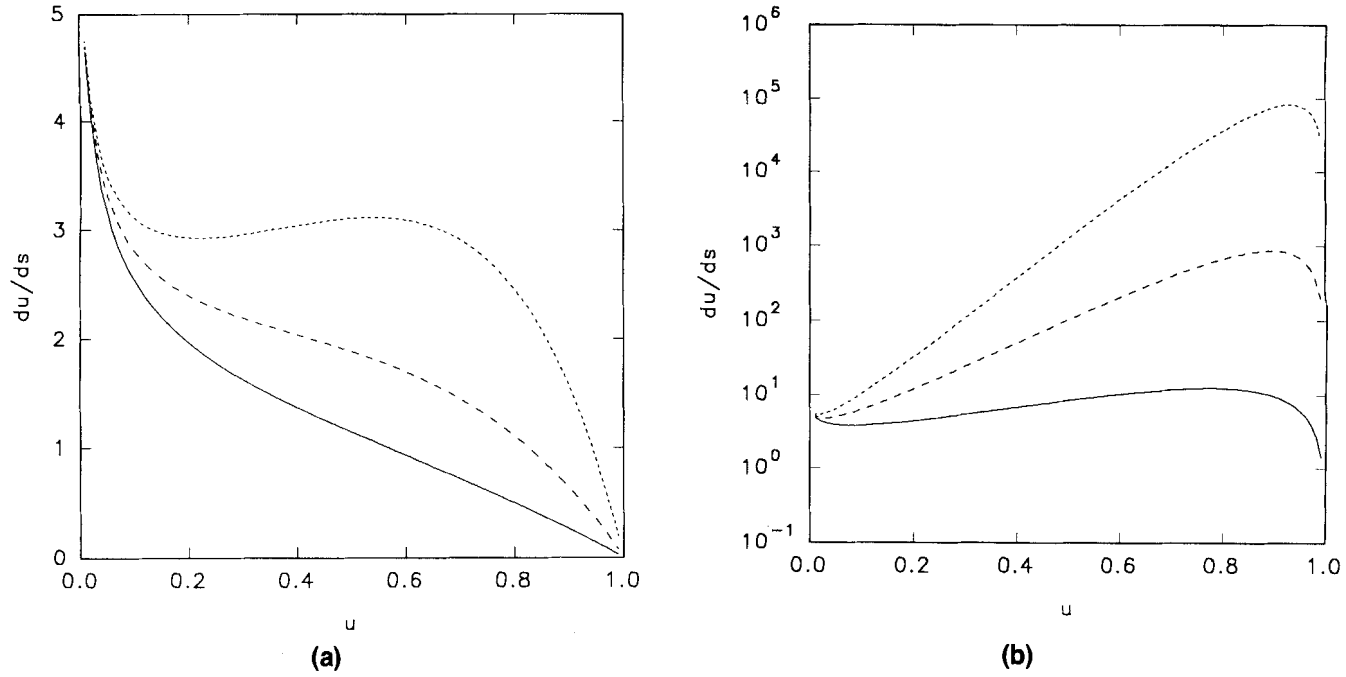

Figure 1. u_s vs. u for various values of M according to Eq. 5.

(a) $M = 1$ (——); $M = 2$ (– – –); $M = 3$ (----); (b) $M = 5$ (——); $M = 10$ (– – –); $M = 15$ (----).

where $\hat{s} = e^M s$. The solution, which is written in the original variables, is

$$E_1(M(1-u)) = e^M s + \hat{s}_o; \quad 1-u \sim O(M^{-1}); \quad M \gg 1 \quad (14)$$

where $\hat{s}_o$ is an integration constant. Equation 14 implies an extremely rapid relaxation to the equilibrium concentration after the logarithmic blowup. This can be seen clearly by considering the asymptotic form of Eq. 14 for $(1-u) \sim o(M^{-1})$, $u \simeq 1 - C(M)e^{-e^M s}$ where $C(M)$ is an M dependent constant. It shows that u achieves its equilibrium value very abruptly after the logarithmic growth begins, within a transcendentally small time scale $s \sim O(e^{-M})$.

Equations 11, 12 and 14 can be patched at the crossover

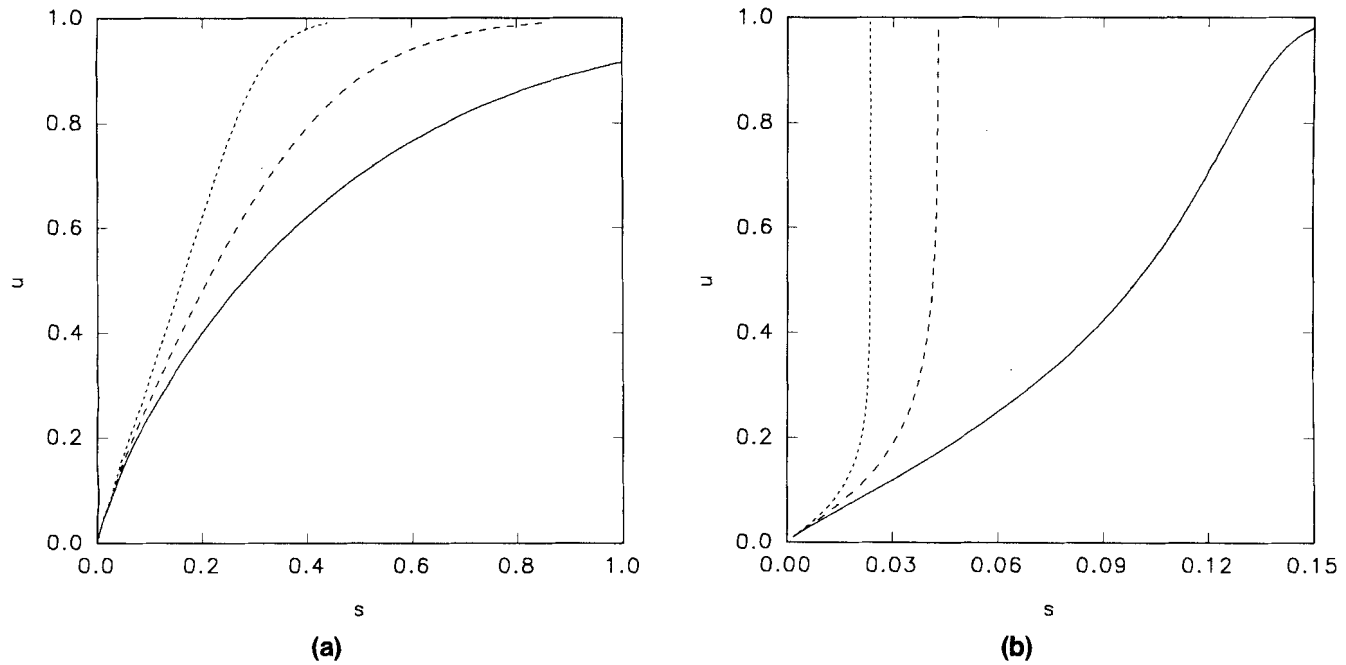

Figure 2. u vs. s for various values of M according to Eq. 10; the lower limit in Eq. 10 was set to 10^{-4} to avoid numerical overflow.

(a) $M = 1$ (——); $M = 2$ (– – –); $M = 3$ (----); (b) $M = 5$ (——); $M = 10$ (– – –); $M = 15$ (----).

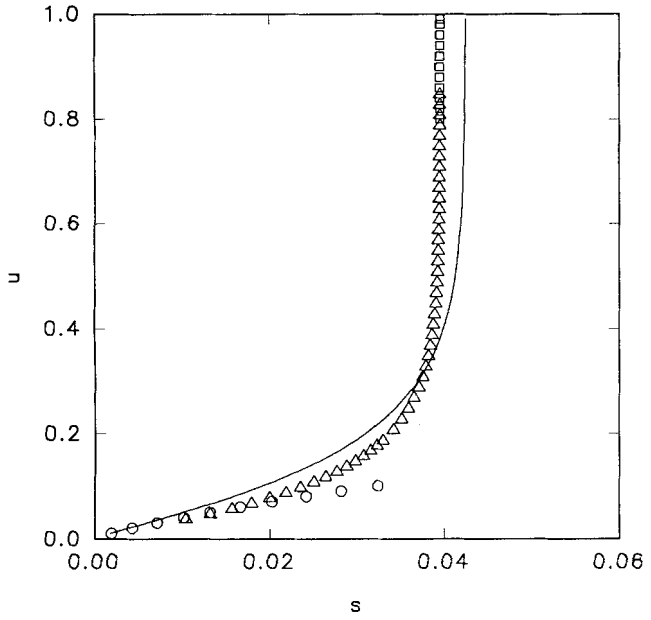

Figure 3. Comparison of exact and asymptotic solutions for u vs. s with $M=10$; asymptotic solutions are patched at the crossover points $u=M^{-1}$ and $u=1-M^{-1}$.

Eq. 10 (——); Eq. 11 (○); Eq. 12 (△); Eq. 14 (□).

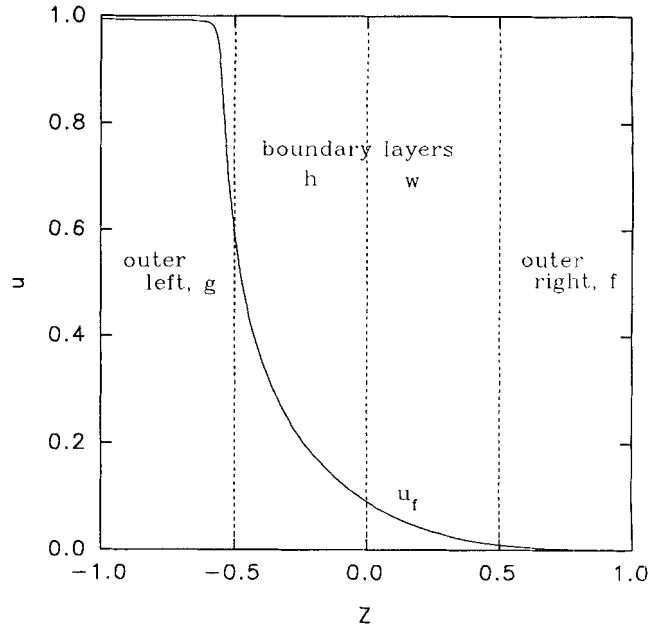

Figure 4. Wave-like concentration profile.

points $u \simeq 1/M$ and $1-1/M$ by appropriate choice of the integration constants $\hat{s}_o$ and $\hat{s}_o$ to give a very good, piecewise-continuous approximation to Eq. 10; Figure 3 shows the comparison for $M=10$.

Perturbation Analysis of Diffusion Equation

We seek a wavelike solution to Eq. 4 for $M \gg 1$ and for time-scales $s > O(M^{-1}/\ln M)$. From numerical studies (Fu and Durning, 1993), we anticipate that the solution has a sharp front where the concentration drops very suddenly over a small spatial scale, from $u \sim O(1)$ on the left to $u \ll 1$ on the right (Figure 4). In seeking a wave-like solution, we apply the transformation $z = x - vs$ where v is the speed of the concentration wave to be determined in the analysis, and expect that the ordinary differential equation governing $u(z)$ submits to a boundary layer analysis.

Under the conditions of interest, the surface boundary condition Eq. 5 can be replaced by

$$u=1 \quad \text{at} \quad x=0 \quad \text{for} \quad 0<s<\infty. \tag{15}$$

Making the transformation $z = x - vs$ in Eq. 4, integrating and making use of the boundary conditions Eqs. 6 and 7 gives

$$vue^{\alpha Mu}(e^{-Mu}u_z)_z - e^{\alpha Mu}u_z - vu = 0 \quad \text{for} \quad -vs < z < \infty. \tag{16}$$

For $M \gg 1$, one sees immediately that in any region where $d/dz \sim O(1)$, i.e., outside the boundary layers, the first term on the left in Eq. 16 representing the effect of memory is negligible compared to the second owing to the coefficient e^{-Mu}.

Auxiliary conditions associated with Eq. 16 can be deduced from the unused auxiliary conditions in the original problem Eqs. 8, 9, and 15. The last gives

$$u=1 \quad \text{at} \quad z=-vs. \tag{17}$$

To state the implications of Eqs. 8 and 9, we must first assign the position $z=0$. Let us define the Case II front position x_f as the location in the fixed coordinates of the peak in π, since it is a precisely defined feature associated with the liquid front [recall the result (v) from numerical work discussed earlier]. Let us also define a characteristic liquid concentration, $u=u_f$, and a characteristic value of $\pi=\pi_f$, corresponding to the front location x_f (Figure 4). Now, $dx_f/ds = v$ which gives $x_f = vs + \text{const}$. Assuming $x_f(0)=0$, i.e., $x_f = vs$ is consistent with Eq. 17, in that both ignore the initial induction process at the polymer/fluid interface, during which the surface concentration relaxes to its equilibrium value. This choice gives $z_f \equiv x_f - vs = 0$. Consequently, $z=0$ corresponds to the location of the liquid front.

With this, Eqs. 8 and 9, imply

$$u=0 \quad \text{for} \quad 0<z<\infty \tag{18}$$

and

$$\pi = -ve^{-Mu}u_z = 0 \quad \text{for} \quad 0<z<\infty. \tag{19}$$

The following subsections examine the dominant balances among the terms in Eq. 16 in several regions. In two outer regions (one for $z>0$ and one for $z<0$), the first term on the left, representing the effect of relaxation on transport, plays a minor role. In the inner, boundary layer regions near $z=0$, this term must be included and is balanced by the second and/or third term on the left, representing transport by ordinary diffusion. Matching at leading order eliminates all unknown integration constants and supplies a formula for v.

It turns out that the preferred matching process employing intermediate limits (Kevorkian and Cole, 1981) cannot be done analytically, and we rely where possible on "patching" the asymptotic solutions, i.e., forcing the values to agree at crossover points.

The numerical work by Fu and Durning (1993) shows that the front speed increases monotically with M [see the result (iv) discussed previously], suggesting $v = v(M)$ diverges with M. The dominant balances depend on the strength of this divergence. It turns out that $v \sim O(M^{1/2})$ is needed for a self-consistent, leading-order solution; we demonstrate this below by a process of elimination.

Outer solutions

Consider the outer right region first (Figure 4). We assume $u \leq O(M^{-1})$ to satisfy Eq. 18 for $M \gg 1$ and so let $u \sim M^{-1}f$ in this region. Equation 16 leads to

$$f = 0 \tag{20}$$

when $M \to \infty$; the outer right region is completely dry. This clearly satisfies Eq. 19.

In the outer left region we know $u \sim O(1)$ by Eq. 17. Let $u \sim g$; neglecting the subdominant first term on the left in Eq. 16 leads to $e^{\alpha M g} g_z + vg = 0$ indicating transport controlled by unsteady ordinary diffusion to the left of the front. Note, however, that the term vg is also negligible when $d/dz \sim O(1)$ since $e^{\alpha M g} \gg 1$. So, to leading order we actually have $e^{\alpha M g} g_z = 0$. The solution, subject to Eq. 17, is

$$g = 1. \tag{21}$$

In deriving this we assumed $d/dz \sim O(1)$, but it is actually valid under the less restrictive assumption that $d/dz > O(ve^{-\alpha M})$. Considering that the extremal value of z occurs at $x = 0$ where $z = -x_f$, the least restrictive condition for which Eq. 21 holds can be stated

$$x_f \sim o(e^{\alpha M}/v). \tag{22}$$

Equation 22 is a solvability condition, needed for a wave-like solution of Eq. 16.

Boundary layer solutions

Now consider the boundary layer regions (Figure 4). Intuition suggests that ordinary diffusion might dominate in a boundary layer adjacent to the outer right. Let $u \sim M^{-1}w$ in this layer. In order for the diffusive terms in Eq. 16 to balance we must scale z by $\tilde{z} = vz$. Then, Eq. 16 becomes

$$\frac{v^2}{M} w e^{\alpha w} (e^{-w} w_{\tilde{z}})_{\tilde{z}} - e^{\alpha w} w_{\tilde{z}} - w = 0. \tag{23}$$

Note that if $v \sim o(M^{1/2})$, then the first term drops out when M diverges and ordinary diffusion dominates. For $v \geq O(M^{1/2})$, one cannot drop the first term and relaxation plays an important role in the layer.

First consider the case $v \sim o(M^{-1/2})$. The leading order solution to Eq. 23 becomes

$$E_1[\alpha M u_f] - E_1[\alpha w] = -\tilde{z}. \tag{24}$$

where the integration constant ensures patching to the front concentration u_f at $z = 0$. Note that $w \to 0$ as $\tilde{z} \to \infty$, so that Eq. 24 matches Eq. 20 on the right. For Eq. 24 to be self-consistent, we must find that π has a maximum and the corresponding value of u $(= u_f)$ has the correct M scaling, i.e., $u_f \leq O(M^{-1})$. From Eq. 24 we find $\pi = v^2 e^{-(1+\alpha)w} w/M$ which does show a maximum; calculating u_f from the condition $\pi_z = 0$ gives

$$u_f = M^{-1}(1+\alpha)^{-1} \tag{25}$$

showing that Eq. 24 is indeed self-consistent. We subsequently consider u_f and the corresponding value of π

$$\pi_f = v^2 u_f / e \tag{26}$$

as righthand boundary conditions on the adjacent lefthand inner balance, in order to patch the left- and righthand boundary layers at $z = 0$.

In a lefthand boundary layer adjacent to the outer left, $u > O(M^{-1})$. One cannot drop the first term on the left in Eq. 16, representing the influence of memory (i.e., of relaxation). Note that whenever $d/dz > O(1)$, then the third term on the left in Eq. 16 can be neglected in comparison with the other two. Denoting by $\bar{z}$ the boundary layer variable and putting $u \sim h$ in this layer, we have

$$vh(e^{-Mh} h_{\bar{z}})_{\bar{z}} - h_{\bar{z}} = 0 \tag{27}$$

as the dominant balance in this region. Equation 27 balances the effects of memory and of quasi-steady ordinary diffusion.

Integrating once leads to

$$e^{-Mh} h_{\bar{z}} = \frac{1}{v} \ln h + \text{constant} = \frac{1}{v} \ln h. \tag{28}$$

Choosing the integration constant as zero, as shown in the second part of Eq. 28, ensures matching to the outer left solution. Note that Eq. 28 is isomorphic to Eq. 5, indicating that the lefthand boundary layer profile has the same shape as the surface concentration's time history. Integrating again leads to

$$\int_{u_f}^{h} \frac{e^{-My}}{\ln y} dy = \frac{\bar{z}}{v} \tag{29}$$

where the integration constant is chosen to patch h and w at $z = 0$. Equations 20, 21, 24, 25 and 29 are the leading-order solutions assuming $v \sim o(M^{1/2})$. They contain the unknown parameter v determined by patching π derived from h and w at $z = 0$. This leads to $v = [e(1+\alpha)M \ln M(1+\alpha)]^{1/2}$, which contradicts the original assumption $v \sim o(M^{1/2})$. Consequently, v must scale $v \geq O(M^{1/2})$.

We now assume $v > O(M^{1/2})$. The outer left solution at leading order remains the same (Eq. 21 subject to Eq. 22) because of the overwhelming effect of the exponential factors in Eq. 16 when $u \sim O(1)$ and $M \to \infty$. For the righthand boundary layer, introduce $\tilde{z} = vz$ and let $w \sim v^{-2}u$; Eq. 16 becomes

$$ww_{\tilde{z}\tilde{z}} - w_{\tilde{z}} - w = 0 \tag{30}$$

at leading order. Integration gives $w_{\tilde{z}} = \ln Ae^{\tilde{z}}w$ where A is an integration constant $\sim O(1)$. There exists a solution such that $w(\tilde{z} \to -\infty) \sim \tilde{z}^2/2$; $w(\tilde{z} \to \infty) \sim e^{-\tilde{z}}/A$, which ensures matching between the right boundary layer and the outer right. This solution displays a maximum in π, allowing calculation of u_f as in the development of Eq. 25. One finds that u_f satisfies $u_f v^2 + \ln Au_f v^2 = 0$ which shows $u_f \sim O(v^{-2})$ consistent with the scaling for w. The corresponding value of π is $\pi_f = -\ln Au_f v^2$. If one proceeds as before to patch π derived from h and w at $z = 0$, the relation $v = A^{-1/2} \sim O(1)$ results. However, this violates the original assumption that $v > O(M^{1/2})$. Attempting a more rigorous matching calculation also leads to a contradiction. Here, we recognize that the function w occupies a doubly infinite domain in $\tilde{z}$ about $z = 0$, and try to match h and w using intermediate limits. This cannot be done directly since w diverges quadratically when $\tilde{z} \to -\infty$ while h approaches a finite value for $\tilde{z} \to 0^-$. The only possibility is to construct an intervening layer, thicker than that for either w or h, which enables matching at either end. Analysis of Eq. 16 shows that it is not possible to construct such a layer. Hence, the assumption that $v > O(M^{1/2})$ must be wrong.

Having reached contradictions assuming either $v \sim o(M^{1/2})$ or $v > O(M^{1/2})$, we conclude $v \sim O(M^{1/2})$. Setting $v = v_o M^{1/2}$ where $v_o \sim O(1)$ leads to the correct dominant balance in the righthand boundary layer. Appropriate scaling for this layer is $\tilde{z} = M^{1/2}z$ and $u \sim M^{-1}w$. Equation 16 becomes

$$v_o we^{\alpha w}(e^{-w}w_{\tilde{z}})_{\tilde{z}} - e^{\alpha w}w_{\tilde{z}} - v_o w = 0 \tag{31}$$

for $M \to \infty$. Since Eq. 31 behaves like Eq. 30 for small w, we know there exists a solution decaying for $\tilde{z} \to \infty$, permitting matching to the outer right. Unfortunately, neither matching or patching of Eqs. 31 and 29 can be done analytically, although numerical matching succeeds, as demonstrated later. One can obtain analytical results however by approximating the concentration profile at the front by a step-exponential shape, as first suggested by Peterlin (1965).

Step-exponential approximation

By adopting two *ad-hoc* mathematical approximations, the boundary layer solutions can be patched at $z = 0$ to find an analytical, leading-order solution consistent with the scaling $v \sim O(M^{1/2})$. First, neglect the logarithmically ascending portion of the concentration profile in the left boundary layer, isomorphic to Eq. 12. Second, drop the first term in Eq. 31, representing relaxation effects in the righthand boundary layer. It turns out that this approximation gives a step-exponential concentration profile for the Case II front.

In deriving the results, it is helpful to note that concentration and nonequilibrium potential at the front are related exactly by

$$\pi_f = v_o^2 M u_f e^{-(\alpha+1)Mu_f}. \tag{32}$$

Now, neglecting the relaxation term in Eq. 31 for $\tilde{z} \geq 0$, we have

$$E_1(\alpha M u_f) - E_1(\alpha w) \simeq -v_o \tilde{z}, \quad \tilde{z} \geq 0 \tag{33}$$

which corresponds to pure diffusion in the right boundary layer; the integration constant in Eq. 33 is chosen to patch to u_f at $z = 0$. Calculating u_f from the maximum in π implied by Eq. 33, and using Eq. 32 to determine π_f therefrom, leads to Eqs. 25 and 26 with $v = v_o M^{1/2}$. We find $u_f \sim O(M^{-1})$, consistent with the scaling assumed for Eq. 31, and $\pi_f \sim O(1)$.

Consider now the lefthand boundary layer governed by Eq. 28. Adopting as the leading-order form the equation isomorphic to Eq. 13 gives

$$E_1[M(1-u_f)] - E_1[M(1-h)] = ze^M/v \tag{34}$$

analogous to Eq. 14, where the integration constant is evaluated to patch h and w at $z = 0$. Note that this neglects the logarithmic portion of the lefthand boundary layer, which is now transcendentally thin. Evaluating π from Eq. 34 and patching π derived from h and w at $z = 0$ leads to $\pi_f = 1 - 1/[M(\alpha+1)] = v_o^2/[e(\alpha+1)]$ which gives

$$v = v_o M^{1/2}; \quad v_o = \sqrt{e(\alpha+1)} + O(M^{-1}). \tag{35}$$

This agrees with the scaling of v assumed for Eq. 31.

Discussion

Consider first the solvability condition Eq. 22 needed for a wave-like solution. Equation 22 corresponds to

$$\frac{V}{D_{ol}/\xi_f} = \frac{\xi_f^2/D_{ol}}{\xi_f/V} \sim o(1) \tag{36}$$

in the dimensional quantities. Here V is the actual speed of the front, ξ_f is its position (in polymer material coordinates), and D_{ol} means the (polymer material) diffusion coefficient in the outer left region, i.e., at the equilibrium concentration c_e. The physical meaning of Eq. 36 is clear: A wave-like solution exists only if the characteristic velocity for fluid diffusion from the reservoir to the front greatly exceeds the front speed, or, equivalently, if the characteristic time for diffusion from the reservoir to the front is negligible compared to the time for the front to reach its present position. In other words, the diffusional resistance to the left of the front must be negligible for Case II to appear.

This condition is consistent with experimental evidence, numerical solution of the TW model and previous analytical modeling efforts. Hopfenberg (1978) and Thomas and Windle (1978, 1982) studied the effect of film thickness on Case II using sorption experiments. In systems showing Case II kinetics, increasing significantly the film thickness caused the front speed to decay with time at long times; Thomas and Windle showed that this decay resulted from the development of gradients in the fluid profile in the swollen layer, i.e.,

with the onset of diffusional limitations behind the front in thick samples. The same authors found temperature to have a similar effect in the poly(methylmethacrylate)/methanol system: Increasing the sorption temperature from 20 to 60°C erased Case II characteristics in 1 mm thick plates. They showed that increasing the temperature greatly increased the front speed relative to the diffusion velocity in the swollen region, causing the rapid onset of severe diffusional limitations behind the front.

The requirement of negligible diffusional resistance behind the front is obvious in numerical solutions of the TW model. Fu and Durning (1993) solved the TW model numerically for integral sorption in thin films. The results showed that the model only predicts Case II if the diffusional resistance in the swollen region remains negligible. Increasing the film thickness (by decreasing the parameter θ to excessively small values) or decreasing the diffusion coefficient behind the front (by using a small value of the parameter K), extinguished Case II characteristics [see the features (i) and (ii) discussed in an introductory section]. Indeed, a number of previous efforts to phenomenologically model the Case II process (Astarita and Sarti, 1978; Hui et al., 1987a,b) recognize this requirement and build it into the modeling. For example, Hui et al. (1987b) solved the TW model for a wave-like profile with the assumption that the diffusion coefficient diverges at a small, critical concentration.

Next, consider the analytical results for the front concentration u_f and the front speed v according to the step-exponential profile approximation Eqs. 25 and 35. Together with Eq. 33, the expression for u_f predicts a shallow, diffusive "foot" or "precursor" of liquid of width $\sim O(M^{-1/2})$ just ahead of a sharp moving front in the nearly dry polymer. The foot becomes *more shallow* as the concentration dependence of the viscosity increases, i.e., as M and therefore v increase. The prediction agrees qualitatively with the results of Hui et al. (1987b). Equation 25 also predicts that u_f decays monotonically as α increases. Recall the parameter α controls the rate of increase in the diffusion coefficient with concentration.

Equation 35 predicts that v is sensitive to the strength of nonlinearities in both the viscosity and diffusion coefficient, since it increases monotonically with both M and α. The prediction for the effect of M is in general agreement with the results by Hui et al. (1987), who predict faster front speeds for larger values of M. Compare the predictions of Eq. 35 with the results of the direct numerical solutions by Fu and Durning (1993). Rescaling v for the case sorption in a finite film and making the replacement $\alpha \rightarrow K/M$ leads to

$$v \equiv Vl/D_o = \theta^{-1/2}[e(M+K)]^{1/2} \tag{37}$$

For fixed values of K and M, Eq. 37 predicts $v \sim \theta^{-1/2}$ in agreement with the numerical data by Fu and Durning (1993). For fixed θ and K, the numerical solutions gave that v increases monotonically with M. Figure 5 shows a comparison between the predictions of Eq. 37 (solid line) and the numerical results (v_c means the front velocity determined by tracking propagation of the steep concentration profiles; v_w means the front velocity calculated from the slope of weight uptake data). The agreement between Eq. 37 and the numerical data is remarkably good considering the approximate nature of the

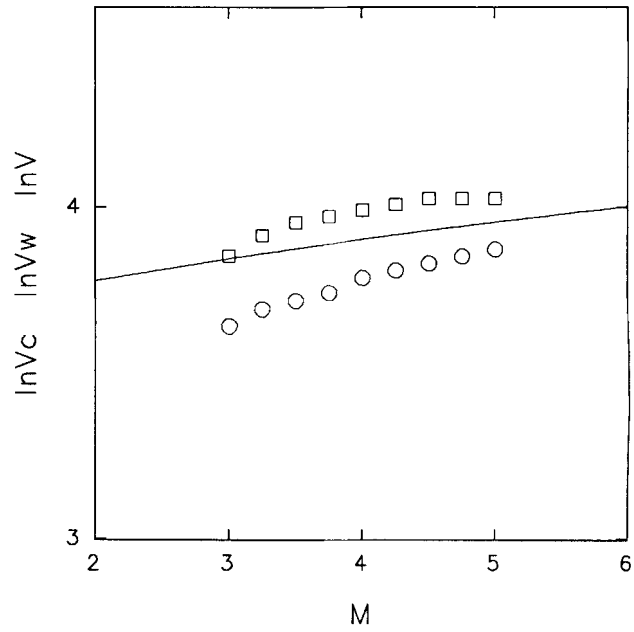

Figure 5. Comparison between the predictions of Eq. 37 and the results of the numerical solutions by Fu and Durning (1993).

v_c (□); v_w (○); predictions of Eq. 37 (——).

formula and that only moderately large values of M were explored in the numerical work.

Before discussing the concentration profiles, consider the dimensional result for the front speed

$$V = \left[\frac{RT}{\varphi_{1e}\bar{V}_1}\right]^{1/2}\left[\frac{D_o}{\eta_o}\right]^{1/2}[e(M+K)]^{1/2} \tag{38}$$

Equation 38 predicts a front speed proportional to the square root of the fluid diffusion coefficient in the dry polymer ahead of the moving front and inversely proportional to the square root of the dry polymer's viscosity. One can predict from dimensional analysis that $V \sim (D*/\eta*)^{1/2}$, where $D*$ and $\eta*$ are characteristic values of the fluid diffusivity and polymer viscosity, respectively (Lasky et al., 1988). Equation 38 supplies definitions of $D*$ and $\eta*$, and gives the numerical prefactor.

Figures 6a–6c show the "exact" and boundary layer profiles, according to Eqs. 16, 25, 33, 34 and 35 for $M = 7$ and $\alpha = 1.0$. Figure 6a shows concentration profiles, Figure 6b shows profiles of the nonequilibrium contribution to the chemical potential π while Figure 6c shows π vs. u. The "exact" solution was determined by a shooting method using the numerical integration of Eq. 16 in the form of a first-order system for u and π by a fully implicit method. Integration was done from right to left with starting values of $u = 10^{-8}$ and $\pi = 0$ and finding v by trial to get $u = 1$ and $\pi = 0$ on the left. The righthand point for beginning the integration was selected by trial to position the peak in π at $z = 0$; this starting position shifted to the right as the starting value of u was reduced, reflecting the existence of a trajectory with u

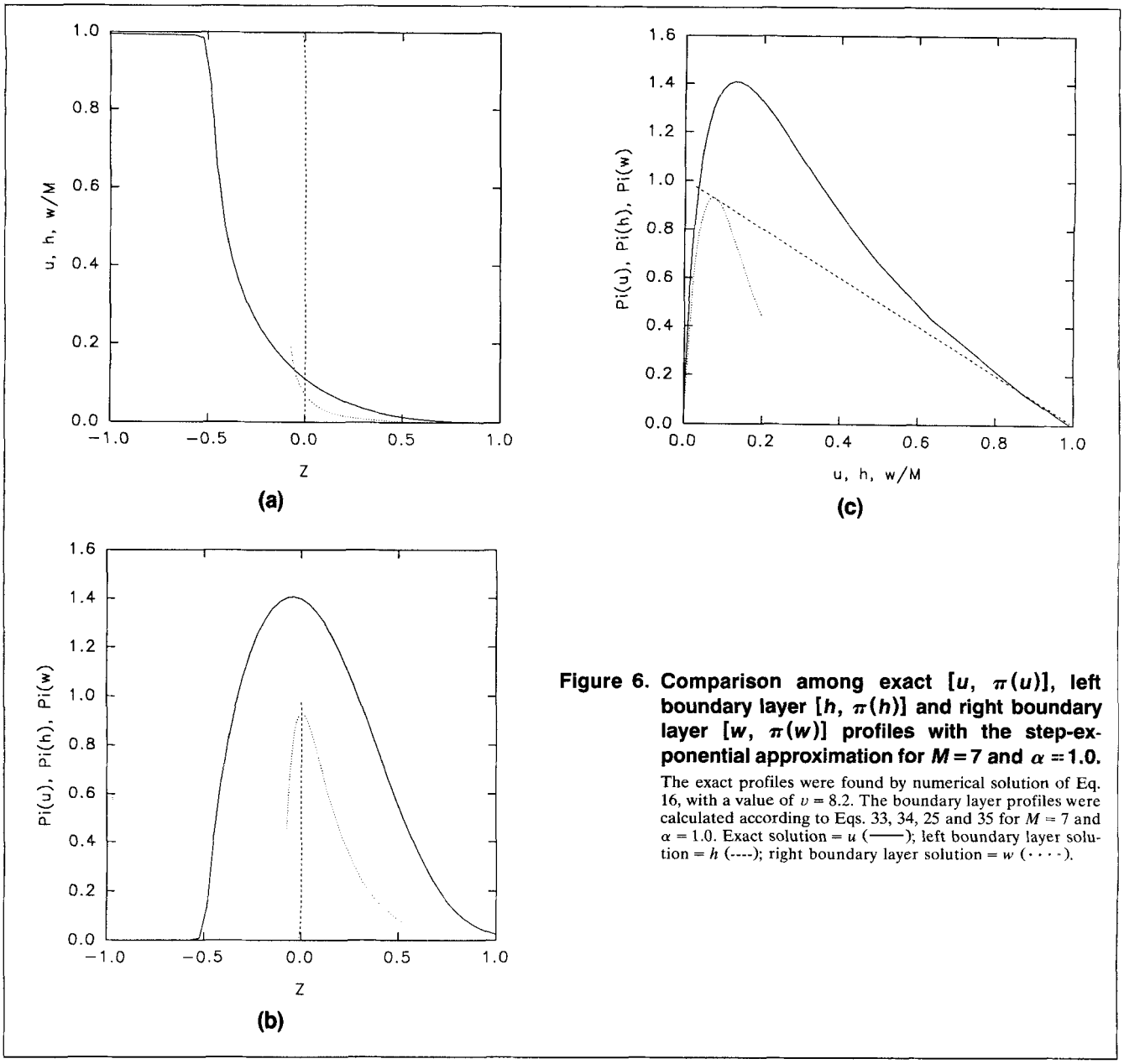

Figure 6. Comparison among exact [u, $\pi(u)$], left boundary layer [h, $\pi(h)$] and right boundary layer [w, $\pi(w)$] profiles with the step-exponential approximation for $M = 7$ and $\alpha = 1.0$.

The exact profiles were found by numerical solution of Eq. 16, with a value of $\upsilon = 8.2$. The boundary layer profiles were calculated according to Eqs. 33, 34, 25 and 35 for $M = 7$ and $\alpha = 1.0$. Exact solution = u (——); left boundary layer solution = h (----); right boundary layer solution = w (· · · ·).

decaying to 0 for $z \to \infty$. The value of υ found for the exact solution in Figure 6 was $\upsilon = 8.2$, above that predicted by Eq. 35 ($= 5.95$ for $M = 7$, $\alpha = 1$). The discrepancy results from the approximations used in getting Eq. 35, mainly that pure diffusion dominates in the righthand boundary layer.

Boundary layer profiles in Figure 6a are a step-exponential approximation. Figure 6 makes it clear that this approximation is *not* a faithful description of the true solution. The lefthand boundary layer profile h is much steeper than the exact solution, because the approximation for h isomorphic to Eq. 14 omits the logarithmically ascending portion of the profile, isomorphic to Eq. 12. The approximate nature of the right boundary layer solution w also appears in Figure 6a where w underpredicts the true solution, and in Figures 6b and 6c where the peak value in π is underpredicted.

Figures 7a to 7c illustrate the boundary layer profiles including the logarithmically ascending portion of h and retaining the relaxation term in w. They compare the solution of Eq. 16 for $M = 7.0$. and $\alpha = 1.0$ with patched asymptotic solutions based on Eqs. 29 and 31 (solved numerically). Patching was accomplished by setting u_f equal to the value determined by the numerical solution of Eq. 16 and setting υ_o to match the values of π_f determined from w and h; this produced excellent agreement between h and w/M at $z = 0$ meaning that patching had been accomplished. Figure 7a shows improved agreement between the exact and asymptotic solutions in both the left- and righthand boundary layers (cf. Figure 6a). Clearly, relaxation effects have an important influence on the shape of the Case II front. Figures 7b and 7c show improvement in the predictions for π compared to the step-exponential approximation (cf. Figures 6b and 6c). Unfortunately, one cannot obtain analytical expressions for u_f, π_f or υ in this case, even when the simple patching process is employed.

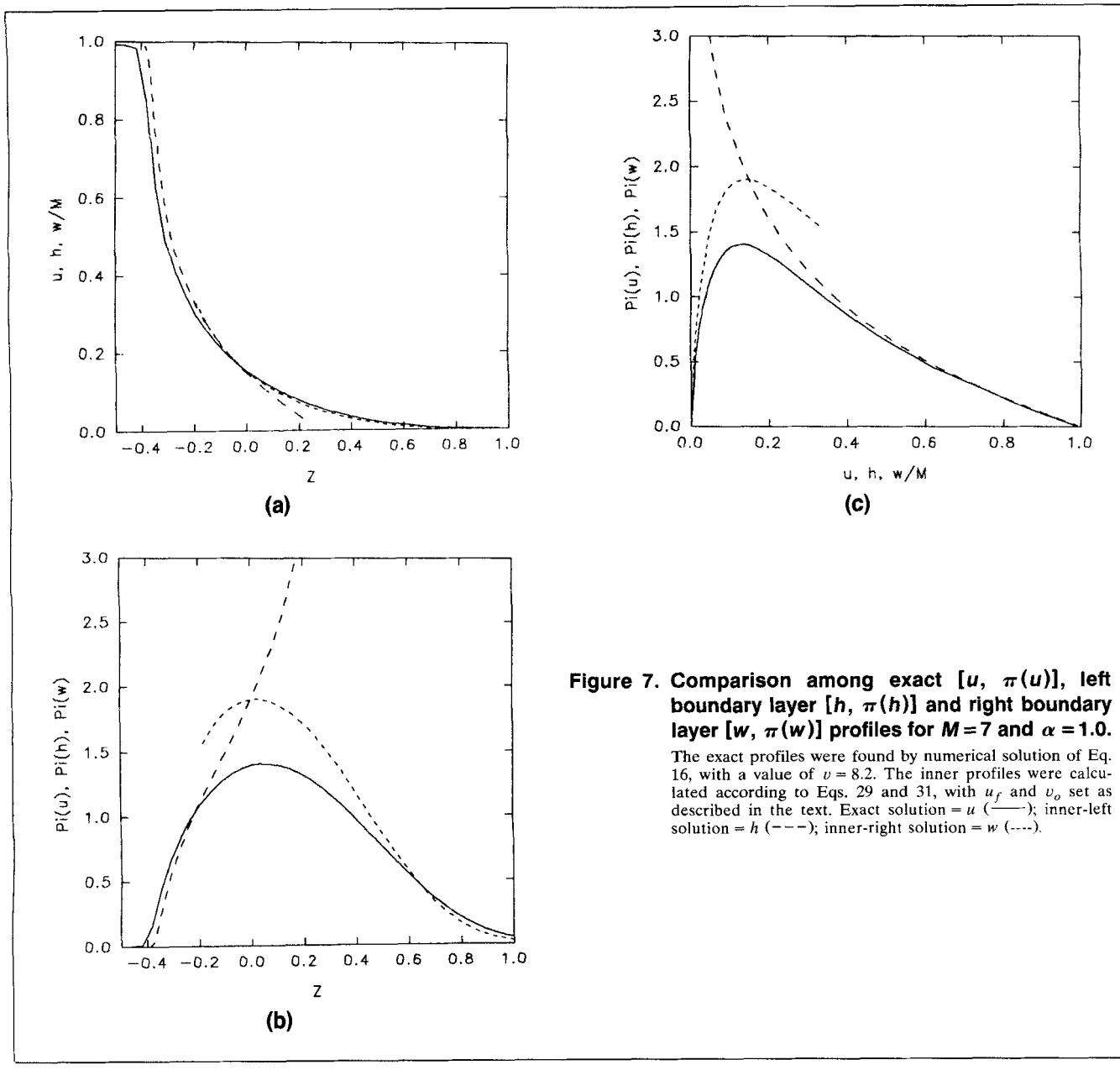

Figure 7. Comparison among exact [u, $\pi(u)$], left boundary layer [h, $\pi(h)$] and right boundary layer [w, $\pi(w)$] profiles for $M=7$ and $\alpha=1.0$.

The exact profiles were found by numerical solution of Eq. 16, with a value of $v=8.2$. The inner profiles were calculated according to Eqs. 29 and 31, with u_f and v_o set as described in the text. Exact solution = u (——); inner-left solution = h (– – –); inner-right solution = w (----).

Conclusion

We analyzed Thomas and Windle's model for Case II transport by a singular perturbation in the parameter $\epsilon = 1/M$, where M controls how quickly the viscosity decays with fluid concentration. The calculation yields a wave-like solution at leading order with two adjacent traveling boundary layers (Figure 4) separating a fully equilibrated outer region on the left (Eq. 21) from a completely dry outer region on the right (Eq. 20). A solvability condition (Eq. 22) is required, which has the physical meaning of negligible diffusional resistance in the equilibrated, left outer region between the fluid reservoir and the moving front. In the lefthand boundary layer, quasi-steady ordinary diffusion balances relaxation (Eq. 27), while in the righthand boundary layer, unsteady ordinary diffusion and relaxation compete (Eq. 31). Unfortunately, the last means that no real simplification occurs in the governing equations at leading order. Consequently, an intermediate-limit matching procedure cannot be carried out to find an explicit formula for the key dynamic feature, the front speed v, although the scaling $v \sim O(M^{1/2})$ clearly results. By two (unjustified) approximations, that relaxation does not contribute in the righthand boundary layer and that the lefthand boundary layer has negligible width, one can find very simple, analytical solutions (Eqs. 33 and 34) which correspond to widely assumed step-exponential concentration profile (Peterlin, 1965). Patching the boundary layers at the moving front gives a simple formula for the front speed with the correct M scaling.

The approximate analytical results agree qualitatively with Hui et al.'s (1987b) analysis of an alternate version of Thomas and Windle's model, where a discontinuous diffusion coefficient was assumed, but are much simpler. Further, the pre-

dictions for v agree with values from full numerical solutions of the original TW model by Fu and Durning (1993) (Figure 5). A comparison between the exact solution of the problem, obtained numerically by a shooting technique, and the step-exponential solution shows that the true profiles are not well represented by the step-exponential. Therefore, analysis of experimentally determined concentration profiles ought to employ the full model. Nonetheless, the step-exponential approximation does supply a result of practical importance: an accurate, accessible formula for the front speed, which is the most important dynamic feature of Case II transport. This result does not rely on the unrealistic simplifying assumptions taken by Hui et al. (1987) and is connected to a first-principles theory by the development in Fu and Durning (1993).

Of fundamental importance, the present analysis, together with previous works (Billovits and Durning, 1990, 1993, 1994; Mehdizahdeh and Durning, 1990; Fu and Durning, 1993), shows that the relatively simple nonequilibrium thermodynamic results by Durning and Tabor (1986) can explain the essential characteristics of the most important experimental manifestations of viscoelastic diffusion in polymer/fluid mixtures: The appearance of "two-stage" weight uptake in linear-perturbation, differential sorption experiments (Billovits and Durning, 1990, 1993, 1994; Mehdizahdeh and Durning, 1990) and the appearance of Case II transport in sufficiently nonlinear, integral sorption experiments (Fu and Durning, 1993). These studies clarify the relationship between two-stage uptake and Case II transport in the context of a first principles development.

Acknowledgment

The authors thank Dr. P. Hagan of the Los Alamos National Lab. and T. Witelski of CALTECH AMA for helpful discussions and acknowledge financial support from the National Science Foundation (grants CTS-89-19665 and DMS-94-07531) and the Air Force Office of Scientific Research (grant AFOSR-91-0045). DSC acknowledges support from the Department of Energy (grant W-7405-ENG-36 at the Center for Nonlinear Studies at Los Alamos) and the Director's Office (T-DO) of the Theoretical Division at Los Alamos. DAE acknowledges support under graduate and postdoctoral fellowships from the NSF and the John and Fannie Hertz Foundation.

Notation

c_f = value of c at moving front
$D_o = D(c = 0)$
D' = mobility scaling the effect of memory in diffusion flux
D'_o = constant defined in Eq. 2
f = leading-order solution to Eq. 16 in the outer right region
g = leading-order solution to Eq. 16 in the outer left region
h = leading-order solution to Eq. 16 in the left boundary layer
k = phenomenological constant in $D(c)$
l = dry polymer film half thickness
m = phenomenological constant in $\eta(c)$
R = gas constant
s = dimensionless time
$\hat{s} = e^M s$
$\hat{s}_o$ = integration constant
t = time
$\bar{u} = uM$
v = dimensionless front speed in semiinfinite medium
v = dimensionless front speed in finite film
w = leading-order solution to Eq. 16 in the right boundary layer
x = dimensionless distance in semiinfinite media
x_f = dimensionless front position
z_f = value of z at moving front (= 0)
$\bar{z}, \tilde{z}$ = dimensionless distance in the boundary layers

Greek letters

$\alpha = K/M$
$\delta = 1 - u$
$\Delta = M\delta$
$\eta_o = \eta(c = 0)$
π_f = value of π at moving front
τ = shear relaxation time
φ_1 = fluid volume fraction
φ_2 = polymer volume fraction

Literature Cited

Alfrey, T., E. F. Gurnee, and W. G. Lloyd, "Diffusion in Glassy Polymers," *J. Poly. Sci. C*, **12,** 249 (1966).
Astarita, G., and G. C. Sarti, "A Class of Mathematical Models for Sorption of Swelling Solvents in Glassy Polymers," *Poly. Eng. Sci.*, **18,** 388 (1978).
Billovits, G. F., and C. J. Durning, "Polymer Material Coordinates for Mutual Diffusion in Polymer-Penetrant Systems," *Chem. Eng. Commun.*, **82,** 21 (1989).
Billovits, G. F., and C. J. Durning, "Two-Stage Weight Gain in the Poly(Styrene)-Ethylbenzene System," *Poly. Commun.*, **31,** 359 (1990).
Billovits, G. F., and C. J. Durning, "Linear Viscoelastic Diffusion in the Polystyrene-Ethylbenzene System: Differential Sorption Experiments," *Macromol.*, **26,** 6927 (1993).
Billovits, G. F., and C. J. Durning, "Linear Viscoelastic Diffusion in the Polystyrene-Ethylbenzene System: Comparison Between Theory and Experiment," *Macromol.*, **27,** 7630 (1994).
Durning, C. J., and M. Tabor, "Mutual Diffusion in Concentrated Polymer Solutions," *Macromol.*, **19,** 2220 (1986).
Fu, T. Z., and C. J. Durning, "Numerical Simulation of Case II Transport," *AIChE J.*, **39,** 1030 (1993).
Gautschi, W., and W. F. Cahill, "Exponential Integral and Related Functions," *Handbook of Mathematical Functions*, M. Abramowitz and I. Stegun, eds., Dover, New York (1965).
Hopfenberg, H. B., "The Effect of Film Thickness and Sample History on the Parameters Describing Transport in Glassy Polymers," *J. Memb. Sci.*, **3,** 215 (1978).
Hui, C. Y., K. C. Wu, R. C. Lasky, and E. J. Kramer, "Case II Diffusion in Polymers: I. Transient Swelling," *J. Appl. Phys.*, **61,** 5129 (1987a).
Hui, C. Y., K. C. Wu, R. C. Lasky, and E. J. Kramer, "Case II Diffusion in Polymers: II. Steady-State Front Motion," *J. Appl. Phys.*, **61,** 5137 (1987b).
Kevorkian, J., and J. D. Cole, *Perturbation Methods in Applied Mathematics*, Springer-Verlag, New York, (1981).
Lasky, R. C., E. J. Kramer, and C.-Y. Hui, "Temperature Dependence of Case II Diffusion," *Polymer*, **29,** 1131 (1988).
Mehdizahdeh, S., and C. J. Durning, "Prediction of Differential Sorption Kinetics Near Tg for Benzene in Polystyrene," *AIChE J.*, **36,** 877 (1990).
Peterlin, A., "Diffusion in a Network with Discontinuous Swelling," *J. Poly. Sci., Poly. Lett.*, **3,** 1083 (1965).
Thomas, N. L., and A. H. Windle, "Transport of Methanol in Poly(methyl methacrylate)" *Polymer*, **19,** 255 (1978).
Thomas, N. L., and A. H. Windle, "A Theory of Case II Diffusion," *Polymer*, **23,** 529 (1982).
Vrentas, J. S., and J. L. Duda, "Diffusion," *Encyclopedia of Polymer Science and Engineering*, Vol. 5, 2nd ed., Wiley, New York (1986).

Manuscript received May 12, 1995, and revision received Sept. 8, 1995.